Available online at www.sciencedirect.com
SCIENCE DIRECT
Journal of Power Sources 157 (2006) 422–429
JOURNAL OF POWER SOURCES
www.elsevier.com/locate/jpowsour

Operation of ceria-electrolyte solid oxide fuel cells on *iso*-octane–air fuel mixtures

Zhongliang Zhan, Scott A. Barnett *

Department of Materials Science and Engineering, 2220 N. Campus Drive, Northwestern University, Cook Hall 2036, Evanston, IL 60208, USA

Received 9 July 2005; received in revised form 10 August 2005; accepted 11 August 2005
Available online 15 September 2005

Abstract

Reduced-temperature solid oxide fuel cells (SOFCs) – with thin $Ce_{0.85}Sm_{0.15}O_{1.925}$ (SDC) electrolytes, thick Ni–SDC anode supports, and composite cathodes containing $La_{0.6}Sr_{0.4}Co_{0.2}Fe_{0.8}O_3$ (LSCF) and SDC – were fabricated and tested with *iso*-octane/air fuel mixtures. An additional supported catalyst layer, placed between the fuel stream and the anode, was needed to obtain a stable output power density (e.g. 0.6 W cm^{-2} at 590 °C) without anode coking. The Ru-CeO_2 catalyst produced CO_2 and H_2 at temperatures <350 °C, while H_2 and CO became predominant above 500 °C. Power densities were substantially less than for the same cells with H_2 fuel (e.g. 1.0 W cm^{-2} at 600 °C), due to the dilute (≈20%) hydrogen in the fuel mixture produced by *iso*-octane partial oxidation. Electrochemical impedance analysis showed a main arc that represented ≈60% of the total resistance, and that increased substantially upon switching from hydrogen to *iso*-octane/air.

Keywords: Solid oxide fuel cells; Catalyst; Hydrocarbons; *iso*-Octane; Partial oxidation

1. Introduction

There has been recent interest in the use of solid oxide fuel cells (SOFCs) in applications for portable power generation [1–3] and Auxiliary Power Units (APUs) for transportation [4]. These applications involve the use of high energy density fuels such as propane, gasoline, diesel, and kerosene, which have two main advantages compared with the hydrogen commonly used in fuel cells. First, the refining and distribution infrastructure for these fuels is well established. Secondly, the energy densities of these fuels are considerably larger than for hydrogen, e.g. 34 MJ l^{-1} for gasoline versus 10 MJ l^{-1} for liquefied hydrogen. Typically, such fuels are reformed to hydrogen-rich mixtures using an external partial oxidation reformer. Especially for smaller-scale applications, it would be useful to do internal reforming in the SOFCs in order to reduce power plant size, weight, and complexity, and to provide a heat source within the stack. In addition, it would be useful to minimize SOFC operating temperature in order to minimize startup time as well as the thermal energy required for startup.

There have been a number of recent examples of SOFCs operating by direct internal partial oxidation (POx) reforming of hydrocarbon fuels. Hibino et al. have reported the use of internal POx reforming of various fuels in single-chamber SOFCs, resulting, e.g. in a power density of 0.24 W cm^{-2} at 550 °C with propane/air mixtures [5]. Internal POx of butane has been reported in micro-tubular SOFCs [2,3], yielding a power density of 0.1 W cm^{-2} at 700 °C. Recently, we reported an output power density of 0.70 W cm^{-2} at 790 °C or 0.38 W cm^{-2} at 690 °C with propane–air mixtures in conventional dual-chamber YSZ-electrolyte anode-supported fuel cells [6]. Ru-CeO_2 layers have been added to SOFCs to catalyze propane partial oxidation at temperatures down to ≈400 °C [7], helping to enable thermally self-sustaining single-chamber SOFC stacks that yielded a power output of ∼350 mW (active area = 1.42 cm^2) at 500–600 °C [8]. However, internal partial oxidation of heavier hydrocarbon fuels,

* Corresponding author. Tel.: +1 847 491 2447; fax: +1 847 491 7820.
E-mail address: s-barnett@northwestern.edu (S.A. Barnett).

0378-7753/$ – see front matter © 2005 Elsevier B.V. All rights reserved.
doi:10.1016/j.jpowsour.2005.08.008

e.g. gasoline and diesel, has not been demonstrated previously.

In this paper, we describe results on the operation of reduced-temperature SOFCs on mixtures of air and *iso*-octane, a common surrogate for gasoline. The cells, which consisted of thin Sm-doped ceria ($Ce_{0.85}Sm_{0.15}O_{1.925}$, SDC) electrolytes with Ni–SDC anode supports, were operated at temperatures ≤600 °C. An additional catalyst layer was utilized in order to obtain stable operation without coking.

2. Experimental

The SOFCs were prepared as follows. Anode powders of SDC (18 $m^2 g^{-1}$, Nextech) and NiO (3.6 $m^2 g^{-1}$, J.T. Baker) in a weight ratio of 60:40 were ball-milled for 20 h with ethanol as the medium, then 10% starch was added and ball-milled for 4 h. The powders were dried at 80 °C, screened with 120-mesh sieve, and pressed into pellets, which were bisque fired at 800 °C for 4 h. A NiO–SDC anode active layer and a thin SDC-electrolyte layer were then colloidally deposited on the NiO–SDC support. The colloidal solutions were prepared by ball-milling the solid powder (SDC electrolyte or NiO–SDC anode) in ethanol containing 1% polyethyleneimine as a dispersant and 3% poly(vinyl butyral)–1% ethyl cellulose as a binder. The thickness of the deposited layer was controlled by the volume of the colloidal solution applied. After co-sintering of the anode/electrolyte at 1400 °C for 6 h, $La_{0.6}Sr_{0.4}Co_{0.2}Fe_{0.8}O_3$ (LSCF)–$Ce_{0.85}Sm_{0.15}O_{1.925}$ (SDC) cathode layers were applied. LSCF–SDC cathode inks were prepared by mixing LSCF powder (6 $m^2 g^{-1}$, Praxair) with SDC powder (NexTech) in a weight ratio of 7:3, and then mixing with a screen-printing vehicle (Heraeus) in a three-roll mill. The cathode ink was printed onto the SDC electrolyte and fired at 1100 °C for 4 h. A second layer of pure LSCF, prepared as noted above, was then applied and fired at 900 °C for 4 h.

The catalyst layers were supported on a porous disc consisting of partially stabilized zirconia (PSZ, 7 $m^2 g^{-1}$, Tosoh) and CeO_2 (15 $m^2 g^{-1}$, Inframat). PSZ and CeO_2 powders in a 50:50 weight ratio were ball-milled with 20% starch for about 24 h. The powders were dried at 80 °C, passed through a 120-mesh sieve, and pressed into pellets that were sintered at 1400 °C for 4 h. RuO_2 (45–70 $m^2 g^{-1}$, Aldrich) and CeO_2 (15 $m^2 g^{-1}$, Inframat) powders in a 1:10 weight ratio were combined in a colloidal suspension with ethanol as the solvent, deposited on both sides of the PSZ–CeO_2, and fired at 900 °C for 4 h to form a 10–20 μm-thick catalyst layer. Fig. 1 shows a low magnification SEM image of a typical catalyst layer, with a porous 0.3–0.4 mm-thick PSZ–CeO_2 support and porous 10–20 μm-thick Ru-CeO_2 catalysts on both sides.

Fig. 2 shows schematically the apparatus used for SOFC electrical testing and mass spectrometer measurements. Single SOFCs were tested in a tube furnace at setpoint temperatures from 300 °C to 600 °C. Ambient air was maintained on the cathode side. At the start of each test, humidified hydrogen was flowed through the anode compartment with the cell at ≈500 °C for ≈12 h, by which time the anode was reduced to Ni–SDC. After baseline testing in humidified hydrogen, testing was done in *iso*-octane/air mixtures obtained by flowing 100 sccm air through a bubbler containing *iso*-octane at 296 K (yielding ≈6.2% *iso*-octane). This corresponded to an O_2 to C_8H_{18} ratio of 3.2, slightly lower than the ideal ratio for partial oxidation of 4. This ratio was used to avoid the flammability range (1–6%) for *iso*-octane–air mixtures. Tests were done both in the conventional geometry, i.e. with no catalyst layer, and with a catalyst layer as shown in Fig. 2. The PSZ–CeO_2 supported catalyst layer and the anode side of the cell were sealed to alumina tubes using Ag ink. Current collector grids were painted on the electrodes using Ag inks. The *I–V* curves and electrochemical impedance spectra (EIS) were obtained using an IM6 Electrochemical Work-

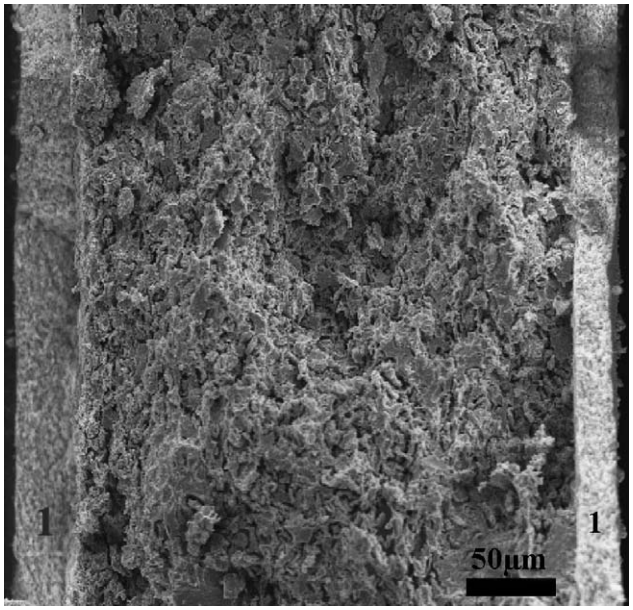

Fig. 1. Fracture cross-sectional SEM micrograph from the catalyst layer, showing both Ru-CeO_2 layers and the PSZ–CeO_2 support, taken after stable SOFC operation in *iso*-octane/air fuel mixtures at 590 °C (1: Ru-CeO_2; 2: PSZ–CeO_2).

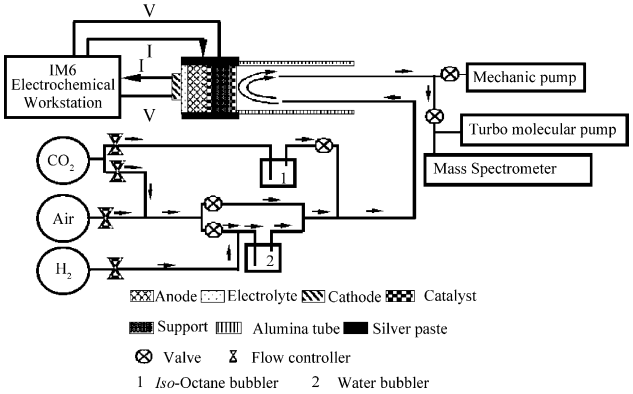

Fig. 2. Schematic illustration of the apparatus used for SOFC electrical testing and mass spectrometer measurements.

station (ZAHNER, Germany). The frequency range for the impedance measurement was 0.1 Hz–100 kHz.

For catalysis measurements, the fuel exhaust gas was analyzed by a differentially pumped mass spectrometer. The catalyst layer was placed against dense YSZ substrates and sealed to alumina tubes using Ag ink, just like in the fuel cell tests. Ar was used in place of nitrogen to facilitate mass spectrometer measurements of the exhaust gas, in particular to avoid the interference between N_2 and CO at mass 28.

The SOFC temperature can increase substantially above the furnace temperature when hydrocarbon–air mixtures are used, due to the heat released by the partial oxidation reaction [6]. We have calibrated the cell temperature by observing changes in the ohmic portion of electrochemical impedance spectra upon switching the fuel from hydrogen to *iso*-octane/air. That is, the temperature was determined via the temperature dependence of the electrolyte resistance. The calibration was done using YSZ-electrolyte SOFCs (unpublished), since the electrolyte resistance measurement is complicated by electronic conductivity in the SDC-electrolyte cells. The measurements indicated that the actual cell temperature was ≈40 °C higher than the furnace temperature. Cell temperature values in the results presented below include this correction.

3. Results and discussion

3.1. Thermodynamic and catalytic considerations

A thermodynamic calculation described previously [6] was used to predict the equilibrium composition of a 6% *iso*-octane–94% air fuel versus temperature T (Fig. 3). The H_2 mole fraction increases with increasing T, while H_2O shows the opposite trend. Similarly, the CO content increases with increasing T, exceeding the gradually decreasing CO_2 content at ≈600 °C. Significant CH_4 is also present, but decreases with increasing T. Finally, coking is predicted at all temperatures for this relatively low O_2 to C_8H_{18} ratio of 3.2, with the C content decreasing from 58% of the input C at 400 °C to 20% at 800 °C.

Although Fig. 3a suggests that the formation of carbon was expected thermodynamically over temperature from 300 °C to 800 °C, no carbon was observed on the catalyst layer by SEM–EDX even after extended exposure to these gas mixtures. The coking was presumably kinetically limited for the Ru-CeO_2 catalyst layer [9]. Thus, a calculation was done where solid carbon was not allowed, potentially better matching the experimental results for the catalyst layers. Fig. 3b shows the gas composition for the same conditions as Fig. 3a but with no C. The main change with C eliminated is that the amount of CH_4 is much increased; methane forms because it is the most stable C-containing species, other than solid carbon, that can form. The formation of CH_4 uses up much of the available hydrogen, resulting in a reduction in the amount of steam produced.

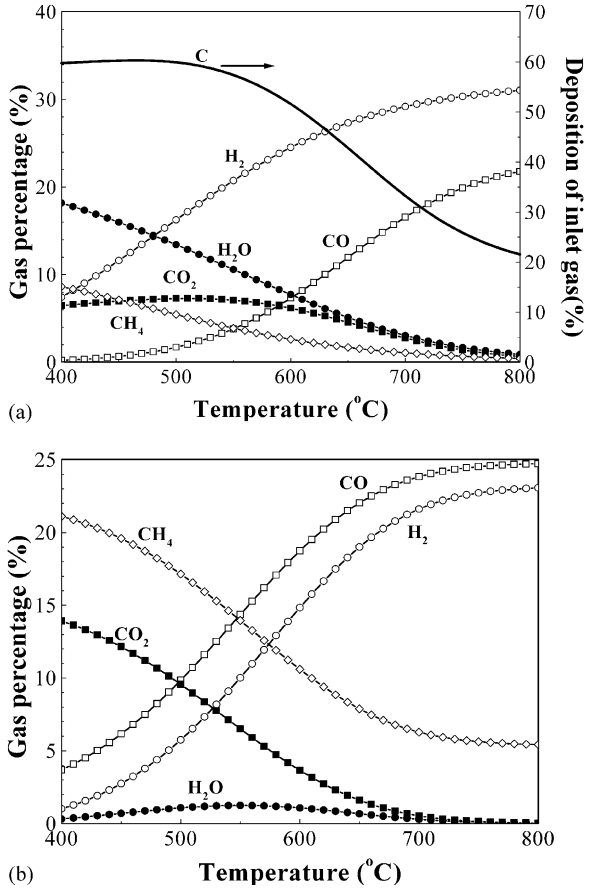

Fig. 3. Thermodynamically predicted equilibrium product distribution as a function of temperature for a 6% *iso*-octane–94% air inlet fuel mixture with carbon formation allowed (a) and not allowed (b).

Fig. 4 shows the mass spectrometry measurements of the exhaust gas composition versus furnace temperature during ramping at a rate of 10 °C min^{-1}, after flowing a 6% *iso*-octane–94% air mixture at 100 sccm over a Ru-CeO_2 catal-

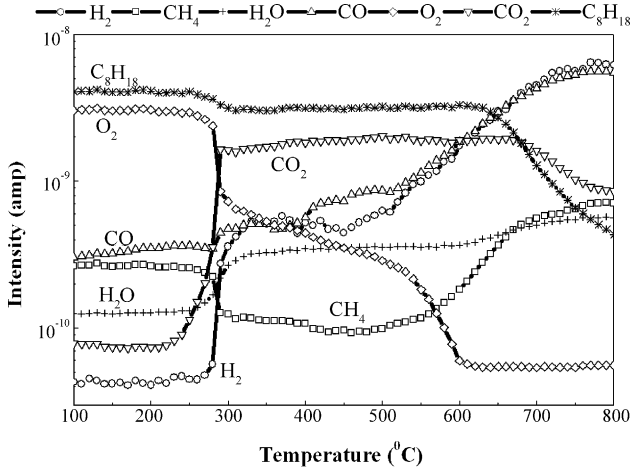

Fig. 4. Mass spectrometer peak intensities vs. T while sampling the exhaust gas from a 6% *iso*-octane–94% air fuel mixture flowed over a Ru-CeO_2 catalyst layer at 100 sccm. The temperature ramp rate was 10 °C min^{-1}.

ysis layer. There was no apparent reaction up to ~280 °C, where the O_2 and C_8H_{18} intensity began to decrease and the CO, CO_2, and H_2 contents increased above the background levels. The O_2 continued to decrease and these products increased until ≈600 °C. The oxygen was entirely consumed by ≈600 °C, but for this gas composition there was still considerable *iso*-octane remaining. The *iso*-octane peak decreased and methane increased as T is increased above 600 °C; note that *iso*-octane accumulated in the gas lines during temperature ramp measurement, making this peak a less reliable indicator than the oxygen peak. Overall, comparison with Fig. 3 indicates that the mixture tends to reach equilibrium at $T > 600$ °C. The CO and H_2 contents continued to increase with increasing T above 600 °C, before saturating above ≈750 °C. This change was due to the shift in equilibrium products from H_2O to H_2 and CO_2 to CO, as shown in Fig. 3. The rapid decrease in the CO_2 peak with increasing T above ≈600 °C provides evidence of this. Similar mass spectrometer results were observed previously for propane–air mixtures with either Ru-CeO_2 catalysts or using the Ni–YSZ anode as the catalyst [6], i.e. there was not a large difference in product selectivity.

Overall, comparison of Figs. 3 and 4 indicates that the measured reaction products agreed reasonably well with the thermodynamic prediction above 550–600 °C, but were limited by reaction kinetics at lower T. The case where no C was allowed (Fig. 3b) showed better agreement with Fig. 4 at higher T, particularly the presence of a strong CH_4 peak. These results show that the conversion of *iso*-octane is incomplete at the temperatures of interest for SDC cells, 500–600 °C. However, this problem would be mitigated in a SOFC stack because there would be a larger catalyst area, and because additional oxygen will be added to the fuel mixture by cell operation. Indeed, it may not be desirable to increase catalyst activity, as this may result in too-fast reforming and localized heating. However, it will likely be useful to develop catalysts that are more selective to CO and H_2. Otherwise, Fig. 3 suggests that at $T < 600$ °C, increasing amounts of H_2O and CO_2 are produced, reducing the potential fuel efficiency.

3.2. Effect of catalyst layer

Attempts to operate the SOFCs on *iso*-octane/air mixtures, without the Ru-CeO_2 catalyst layer, did not yield stable performance. The cell performance was initially good, but the terminal voltage at 0.8 A/cm^2 decreased by ≈37% over 23 h, as shown in Fig. 5. Subsequent visual observation indicated the degradation was due to severe coke buildup on the Ni–SDC anode. This was confirmed by the SEM–EDX spectrum in Fig. 6. Fig. 7a, the cross-sectional SEM image of the cell anode, indicated a major change in the anode microstructure, due to infiltration of solid carbon in a 170-μm-thick layer at the Ni–SDC anode-free surface. A magnified image of the altered layer (Fig. 7b) shows significant white contrast (carbon) that is not present in Fig. 7c, taken from the anode near

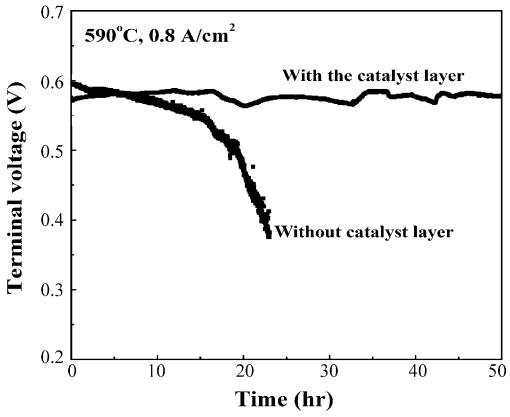

Fig. 5. Life tests results from SOFCs operated on 6% *iso*-octane–94% air at 100 sccm with or without catalyst layers at 590 °C.

the electrolyte. The structure in Fig. 7c is un-altered—similar to that observed for anodes tested in hydrogen.

With the addition of a porous supported catalyst layer between the fuel stream and the anode, the cell's stability was significantly improved. Particularly, a 60-h life test was run at 590 °C on *iso*-octane carried by 100 sccm air (Fig. 5). A constant power output of ~0.46 W cm^{-2} was achieved. No coking was observed on the catalyst layer or the Ni–SDC anode after the tests, as shown in the SEM–EDX results in Fig. 8. The C EDX peak is at the detection limit, and the SEM microstructure appears identical to that from a cell tested in hydrogen.

The catalyst layer effect on SOFC stability can be explained with the aid of the schematic illustration shown in Fig. 9. Carbon did not deposit on the Ru-CeO_2 catalyst layer, despite conditions that favored coking, presumably due to the much lesser tendency of Ru for coking [9]. Coking is also suppressed by electrochemical reaction products at high current densities [10]. On the other hand, the Ru-containing catalyst layer provided good catalytic activity for *iso*-octane reforming. The fast reforming reactions at the catalyst layer substantially reduced the hydrocarbon species in the reformate before reaching the Ni–SDC anode, thereby suppressing

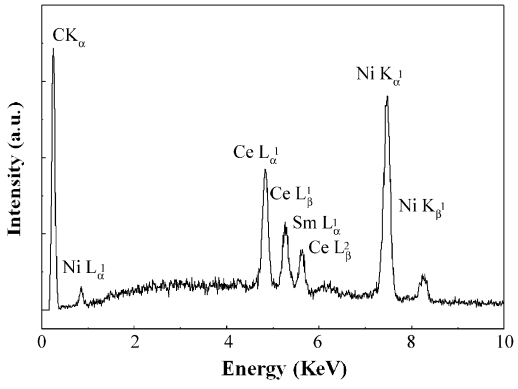

Fig. 6. SEM–EDX spectra taken from the anode surface after degradation in *iso*-octane/air fuel mixtures at 590 °C.

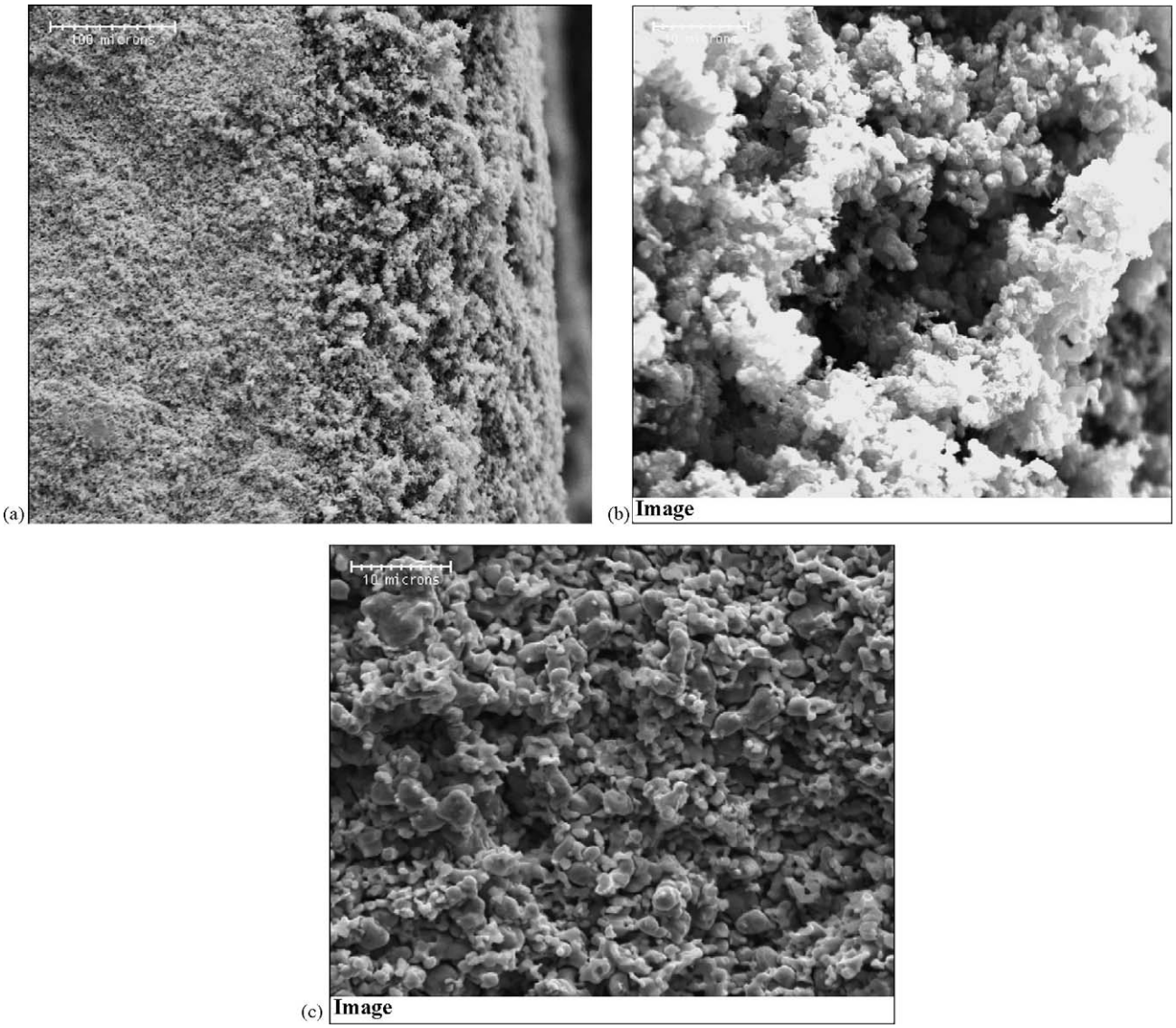

Fig. 7. Cross-sectional SEM micrographs taken from the anode after degradation in *iso*-octane/air fuel mixtures at 590 °C, including (a) a low magnification image of the anode cross-section, and high magnification images of the anode cross-section from a region (b) near the anode-free surface or (c) near the electrolyte.

coking. This is illustrated in the schematic gas concentration gradients in Fig. 9. The figure also illustrates that the H_2 and CO reaction products are at a maximum at the catalyst layer, decreasing in either direction due to electrochemical oxidation at the electrolyte and diffusion into the gas stream. Note that the close proximity of anode and catalyst will tend to couple catalytic and electrochemical reactions, e.g. H_2/CO consumption and H_2O/CO_2 production by the cell will tend to shift the system towards producing more H_2 and CO.

3.3. Cell performance with catalyst layer

Fig. 10 shows an example of the cell performance with *iso*-octane/air fuel with the catalyst layer. Good stability was achieved for this fuel composition, as demonstrated in Fig. 5. A comparison of open circuit voltages (OCVs) and peak *P*-values, for SOFC operation in *iso*-octane/air and pure hydrogen, is shown in Fig. 11. Thermodynamically predicted OCV values based on humidified hydrogen or the equilibrium mixed-gas fuel compositions (Fig. 3) are also shown in Fig. 11. Measured OCV values in humidified hydrogen were 0.8–0.9 V, much lower than the predicted values of ≈1.1 V. This behavior is typical for mixed-conducting SDC electrolytes, although these values are lower than reported by Xia et al. [11,12] and Doshi et al. for thick SDC-electrolyte cells [13]. This is presumably explained by a higher electronic leakage current for the present thinner electrolytes [14].

Power values with *iso*-octane/air and hydrogen were similar at lower *T*, but at higher *T* the power values with *iso*-octane/air were significantly lower. This was probably due to the relatively low hydrogen content in the reformed *iso*-octane/air fuel. The H_2 partial pressure was predicted to

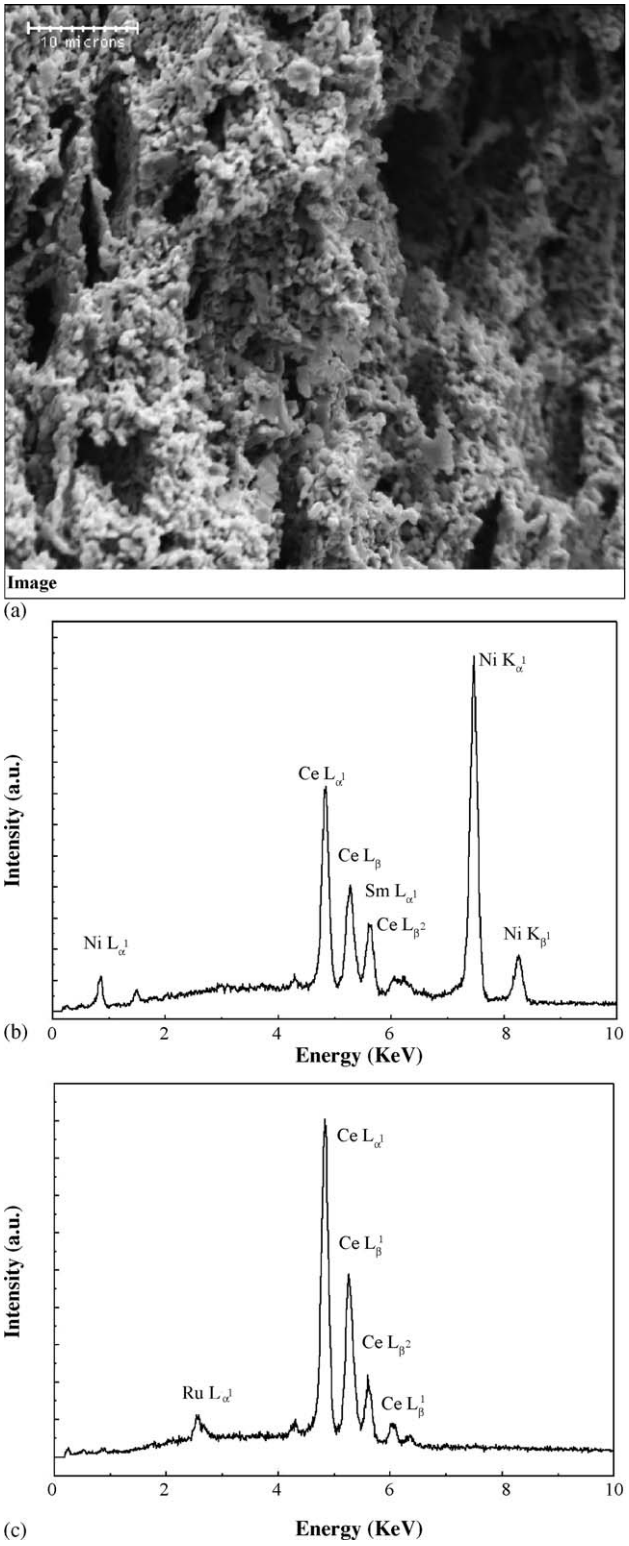

Fig. 8. Fracture cross-sectional SEM micrographs from the anode (a) and EDX spectra taken from (b) the anode or (c) the catalyst layer after stable SOFC operation in *iso*-octane/air fuel mixtures with an addition catalyst layer at 590 °C.

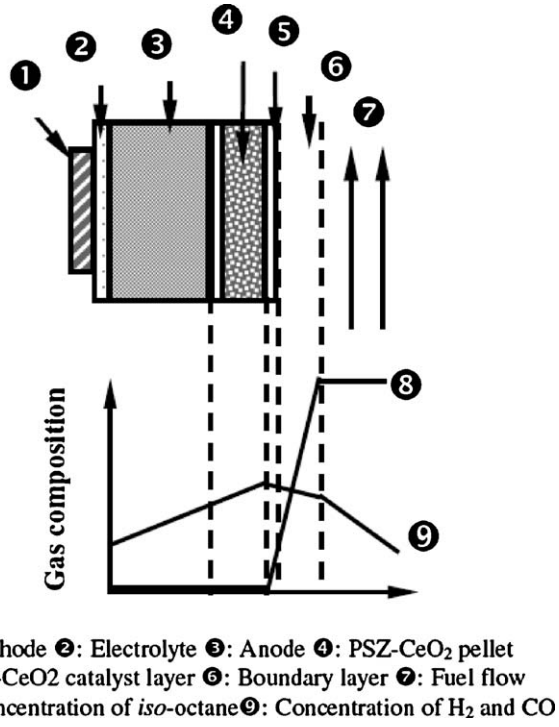

Fig. 9. Simplified schematic illustration of how reactant and product gas concentrations are expected to vary with position for internal reforming SOFCs with a catalyst layer.

be ≈20% at equilibrium (Fig. 3), but the actual value was likely lower due to incomplete catalysis at low temperatures (Fig. 4). Similar behavior was reported previously for SOFCs operated on propane–air mixtures, where the H_2 partial pressure in the reformed fuel was low, ≈20% [6]. The low hydrogen content gives rise to a limiting current that reduces the maximum power density—this can be seen clearly in Fig. 12, which shows the *I–V* curve for *iso*-octane/air (590 °C, 30% fuel utilization at short circuit) in comparison to that for humidified hydrogen (600 °C, 12% fuel utilization at short circuit). Nonetheless, the

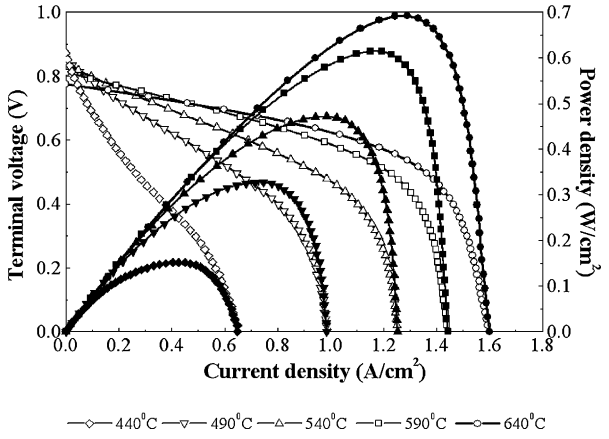

Fig. 10. Voltage and power density vs. current density for the cell with a separate catalyst layer tested with 6% *iso*-octane–94% air at 100 sccm in the anode and ambient air in the cathode at different cell temperatures.

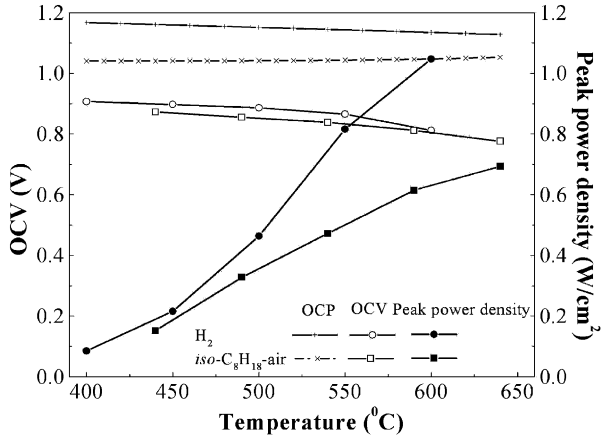

Fig. 11. Open circuit voltage and maximum power density vs. temperature for a cell with a catalyst layer operated with 6% *iso*-octane–94% air or humidified hydrogen at 100 sccm in the anode, and ambient air in the cathode.

maximum power densities with *iso*-octane/air ranged from 0.15 W cm^{-2} at 440 °C to 0.6 W cm^{-2} at 590 °C. These results suggest that the *iso*-octane/air cell performance can be improved by improving the catalyst layer, i.e. activity and selectivity to H_2, and increasing anode porosity.

Fig. 13 shows typical electrochemical impedance spectra at open circuit from a SOFC at (A) high and (B) low temperature. Each plot compares two fuels: humidified hydrogen at 100 sccm and *iso*-octane/air at 100 sccm. At ≈600 °C, the Nyquist plots consisted of a large higher-frequency depressed arc and a small lower-frequency arc. With decreasing temperature, the higher-frequency depressed arc increased, while the lower-frequency disappeared, for example, at ≈450 °C in Fig. 13B. Both arcs were generally larger for *iso*-octane/air than hydrogen, while the high-frequency intercept changed little with fuel as expected (the slight shift was explained by the slightly different cell measurement temperatures). One possible explanation is that the high-frequency arc corresponds to a combination of the anode and cathode polarization, while the low-frequency arc is associated with a gas

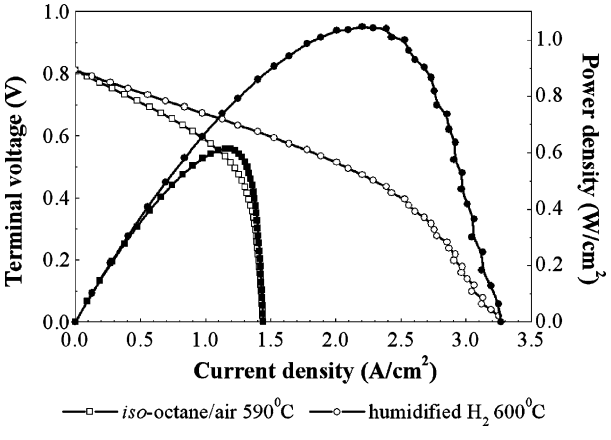

Fig. 12. Comparison of the SOFC *I–V* curve of the cell with a catalyst layer operated with 6% *iso*-octane–94% air or humidified hydrogen at 100 sccm in the anode, and ambient air in the cathode at ≈600 °C.

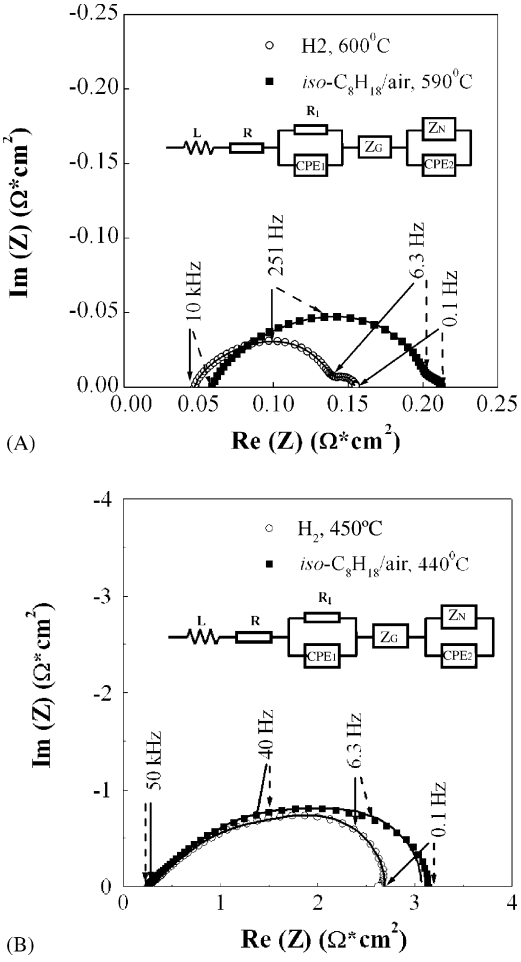

Fig. 13. Nyquist plot of the electrochemical impedance spectroscopy results from a cell at open circuit at (A) high and (B) low temperatures. Each plot compares the cell in humidified H_2 fuel at 100 sccm and 6% *iso*-octane–94% air at 100 sccm. The figure also shows fits to results and the equivalent circuit used, with the elements—*L*: inductance from the connecting wires; *R*: pure ohmic resistance; R_1: anode polarization resistance; Z_G: Gerischer impedance; Z_N: Nernst diffusion impedance; CPE_1 or CPE_2: constant phase elements.

diffusion process. Although the gas diffusion effect is important at high current density as shown in Fig. 12, it is less important at open circuit, so attributing the small EIS arc to diffusion is reasonable.

Quantitative analysis of the EIS results is complicated by the asymmetrical geometry of the anode-supported SOFCs [15] and the mixed electrolyte conductivity [16]. Thus, we only present a brief semi-quantitative discussion here. Fig. 13 also shows fits to the EIS data obtained using the equivalent circuit shown in the inset. Note that the pure ohmic resistance from impedance was slightly lower than expected for a SDC electrolyte, e.g. 0.039 Ω cm^2 versus 0.048 Ω cm^2 at 600 °C, or 0.51 Ω cm^2 versus 0.58 Ω cm^2 at 400 °C [17]. This is reasonable given that the anode side of the SDC-electrolyte is exposed to hydrogen, leading to an increased electronic conductivity. Values from the EIS fits indicated that the interfacial polarization dominated the total cell resistance, e.g.

70% at 590 °C and 90% at 490 °C, in agreement with prior results [11]. Improved electrode performance is thus required to extend SOFC operation to still lower temperature.

4. Summary and conclusions

Operation of Ni–SDC anode-supported SOFCs directly on *iso*-octane/air fuel mixtures was studied. Detailed SOFC electrical testing and electron microscopy clearly showed that conventional SOFCs degraded rapidly due to excessive anode coking, whereas stable coke-free operation was achieved with the addition of a Ru-CeO_2 catalyst layer. This is despite the use of fuel mixtures with compositions expected to yield coking according to equilibrium predictions. Product gas analysis showed the effectiveness of the Ru-CeO_2 catalyst layer for reforming *iso*-octane. The SOFCs with catalyst layer provided high power densities, e.g. 0.6 W cm^{-2} at 590 °C. This internal reforming catalyst layer method provides an alternative to direct-hydrocarbon SOFCs [18]; one advantage of the present method is that novel anodes are not needed to minimize coking problems, such that conventional high-performance SOFCs can be used.

The choice of operating temperature for these SOFCs involves trade-offs. On the one hand, operating temperatures <600 °C yield higher open circuit voltage and less energy loss from internal short circuiting in the mixed-conducting SDC electrolyte. Lower temperature is also beneficial for smaller-scale and transportation applications, where frequent cycles between the cold state and operating temperature are expected. On the other hand, temperatures >500 °C yield higher power densities, and the present results suggest that more complete conversion of *iso*-octane to H_2 and CO is expected at higher temperature. Thus, the optimal operating temperature range for these SOFCs is expected to be in the range 500–600 °C.

Acknowledgements

The authors gratefully acknowledge the financial support of the Defense Advanced Research Projects Agency, funded via California Institute of Technology, during the course of this work. The authors thank Dr. Yi Jiang for describing the colloidal "drop coating" technique used for depositing the electrolyte layers.

References

[1] K. Hayashi, O. Yamamoto, H. Minoura, Solid State Ionics 132 (2000) 343–345.
[2] K. Kendall, M. Palin, J. Power Sources 71 (1998) 268–270.
[3] N.M. Sammes, R.J. Boersma, G.A. Tompsett, Solid State Ionics 135 (2000) 487–491.
[4] S. Mukerjee, M.J. Grieve, K. Haltiner, M. Faville, J. Noetzel, K. Keegan, D. Schumann, D. Armstrong, D. England, J. Haller, in: S.C. Singhal, H. Yokokawa (Eds.), Proceedings of the 7th International Symposium on Solid Oxide Fuel Cells, The Electrochemical Society, Pennington, 2001, pp. 173–179.
[5] T. Hibino, A. Hashimoto, T. Inoue, J. Tokuno, S. Yoshida, M. Sano, Science 288 (2000) 2031–2033.
[6] Z. Zhan, J. Liu, S.A. Barnett, Appl. Catal. A: Gen. 262 (2004) 255–259.
[7] Z. Zhan, S.A. Barnett, Solid State Ionics 176 (2005) 871–879.
[8] Z. Shao, S. Haile, J. Ahn, P. Ronney, Z. Zhan, S. Barnett, Nature 435 (2005) 795–798.
[9] A.T. Ashcroft, A.K. Cheetham, M.L.H. Green, P.D.F. Vernon, Nature 352 (1991) 225–226.
[10] Y. Lin, Z. Zhan, J. Liu, S.A. Barnett, Direct operation of solid oxide fuel cells with methane fuel, Solid State Ionics 176 (2005) 1827–1835.
[11] C.R. Xia, F.L. Chen, M.L. Liu, Electrochem. Solid State Lett. 4 (5) (2001) A52–A54.
[12] C.R. Xia, M.L. Liu, Solid State Ionics 144 (3–4) (2001) 249–255.
[13] R. Doshi, V.L. Richards, J.D. Carter, X.P. Wang, M. Krunmpelt, J. Electrochem. Soc. 146 (1999) 1273–1278.
[14] M. Gödickemeier, K. Sasaki, L.J. Gauckler, in: Bernt Thorstensen, European Fuel Cell Group Ltd. (Eds.), Proceedings of the 2nd European Solid Oxide Fuel Cell Forum, Oslo, Norway, 6–10 May 1996, pp. 717–726.
[15] S.B. Adler, J. Electrochem. Soc. 149 (2002) E166–E172.
[16] M.L. Liu, H.X. Hu, J. Electrochem. Soc. 143 (1996) L109–L112.
[17] Fuel Cell Materials, http://www.nextechmaterials.com/files/Cerias.pdf.
[18] S.A. Barnett, Direct hydrocarbon solid oxide fuel cells, in: W. Vielstich, A. Lamm, H. Gasteiger (Eds.), Handbook of Fuel Cells, vol. 4, Wiley, Hoboken, NJ, 2003, pp. 1098–1108.